



Sub-100 nm patterning of TiO₂ for the regulation of endothelial and smooth muscle cell functions

Journal:	<i>Biomaterials Science</i>
Manuscript ID:	BM-ART-06-2014-000212.R1
Article Type:	Paper
Date Submitted by the Author:	03-Jul-2014
Complete List of Authors:	<p>Muhammad, Rizwan; A*STAR (Agency for Science, Technology and Research), Institute of Materials Research and Engineering; National University of Singapore, Department of Biomedical Engineering</p> <p>Lim, Su Hui; A*STAR (Agency for Science, Technology and Research), Institute of Materials Research and Engineering; National University of Singapore, Electrical & Computer Engineering</p> <p>Goh, Seok Hong; National University of Singapore, Department of Biomedical Engineering; A*STAR (Agency for Science, Technology and Research), Institute of Materials Research and Engineering</p> <p>Bee Khuan, Jaslyn; A*STAR (Agency for Science, Technology and Research), Institute of Materials Research and Engineering</p> <p>Saifullah, M S M; A*STAR (Agency for Science, Technology and Research), Institute of Materials Research and Engineering</p> <p>Ho, Ghim; National University of Singapore, Electrical & Computer Engineering</p> <p>Yim, Evelyn; National University of Singapore, Department of Biomedical Engineering</p>

ARTICLE

Cite this: DOI: 10.1039/x0xx00000x **Sub-100 nm patterning of TiO₂ film for the regulation of endothelial and smooth muscle cell functions**

R. Muhammad,^{a,b,#} S. H. Lim,^{b,e,#} S. H. Goh,^{a,b} J. B. K. Law,^b M. S. M Saifullah,^b G. W. Ho,^e and E. K. F. Yim^{a,c,d*}

Received 00th January 2012,
Accepted 00th January 2012

DOI: 10.1039/x0xx00000x

www.rsc.org/

Previous studies have shown that fundamental cell functions such as adhesion, proliferation, and morphology are regulated by the interaction of cells with basement membrane nano- and micron scale surface topography. By taking basement membrane as a guiding principle, surface can be designed with biophysical cues in the form of surface topographies to modulate cellular functions of vascular endothelial and smooth muscle cells, which are crucial for vascular diseases. Titanium-based materials whose surface is covered by a thin layer of titanium dioxide (TiO₂) are utilized in several regenerative medicine applications such as vascular prosthetics. The utilization of TiO₂-covered materials makes it essential to understand the interaction of cells with the TiO₂ layer to control the cell response. While patterned micro- and nano-topography has shown to regulate important cell functions on non-metallic materials, it would be of interest in the field of regenerative medicine to study cell response on patterned TiO₂ surface layer. Previous studies have mostly focused on studying the cell response on random micro- and nano-roughened metallic and metal oxide surfaces as it is challenging to fabricate patterned TiO₂ surface layer. Here, the biocompatibility of a method that is capable of rational patterning of continuous TiO₂ surface layer with sub-100 nm resolution scale using thermally curable resin-based nanoimprinting is studied. The responses of human umbilical vein endothelial cell (HUVEC), such as proliferation, morphology and focal adhesions, and smooth muscle cell (SMC) proliferation and morphology to the nano-patterned TiO₂ layer were investigated. Overall, TiO₂ layer with surface nano-gratings showed enhanced proliferation of HUVEC, while it significantly lowered the proliferation of SMCs as compared to unpatterned control. The HUVECs and SMCs are shown to be sensitive to the 70 nm gratings as evident by the regulation of proliferation and cell shape by the topography. In HUVECs, significantly lower focal adhesion density was found on TiO₂ nano-gratings, while significantly higher average focal adhesion size of HUVECs was seen on TiO₂ nano-wells and nano-gratings, compared to unpatterned controls.

1. Introduction

Endothelial cells reside on basement membrane which provides biophysical cues in the form of nano- and micro-topography to modulate cell functions¹. Biophysical cues such as surface patterning is an important paradigm to control cell functions through cell-surface interactions by designing improved substrates that interact with these cells.² Several clinical interventions such as the implantation of vascular stents,³ and heart valve⁴ involve the direct cell-surface interactions so the biophysical control of the cell's behaviours will also benefit vascular diseases applications.

Vascular endothelial and smooth muscle cell response studies on well-designed and lithographically micro- and nano-patterned polydimethylsiloxane (PDMS) surfaces have been shown to regulate cell alignment, proliferation, morphology and adhesion,⁵⁻⁸ showing the significance of topographical regulation on the vascular cell behaviors. Metallic and metal oxide material surface modification with random micro- and nano-structured biophysical cues has also been an important research paradigm to modulate cell functions.⁹⁻¹³ However, previous studies have mostly focused on micro- and nano-roughened metallic surfaces produced *via* grit blasting, chemical etching, chemical vapor deposition (CVD), and

physical vapor deposition (PVD) methods,¹⁴ which are limited to produce random surface roughness due to the intrinsic nature of fabrication route. On the other hand, spatially arranged micron and sub-micron titanium features have been demonstrated to modulate vascular cell behaviors.^{15, 16} Among the various choices of metallic materials, titanium-based alloys are the promising candidates for vascular intervention applications because of their excellent corrosion resistance, biocompatibility and mechanical properties¹⁷⁻¹⁹ where corrosion resistance and biocompatibility is mainly contributed by the TiO₂ passivation layer.²⁰⁻²² Thin layer of TiO₂ has also been shown to improve blood compatibility when coated on stainless steel.²³ Very limited research reported the cell-topography interaction studies with rationally designed nano-patterned TiO₂ surface layer. The patterning resolution is limited as previous studies used mask-based lithography and micromachining techniques to fabricate the oxide surface features. The *in vitro* studies using the ordered micro- or nanopatterns on TiO₂ layer for controlling the endothelial and smooth muscle cell response are essential for our fundamental understanding of the cell behaviours for vascular diseases applications, but they are currently hampered by the technological challenges of lithographic patterning of rationally designed features on clinically relevant metal oxide layer. Thus, developing effective biocompatible methods for making nanopatterned metal oxide surfaces with well-defined feature size becomes crucial for the improvement of current clinical interventions that utilize cell-surface interactions.

We have previously demonstrated the fabrication of very high-resolution nanostructures on TiO₂ layer by thermally-polymerizable²⁴ and photo-polymerizable²⁵ titanium dioxide liquid precursors by using nanoimprint lithography. Although the method is versatile with the capability of high-resolution patterning, the biocompatibility of the TiO₂ layer obtained from thermally-polymerizable TiO₂ resin has not been demonstrated. The primary goal of this study is to analyze the biocompatibility and cytotoxicity of TiO₂ surface layer produced *via* heat-treatment of thermally-polymerizable TiO₂ resin and evaluate the effect of two different nano-topographies on the proliferation, morphology, and focal adhesions of vascular endothelial cells. As it is essential to reduce the proliferation of smooth muscle cells¹³ for effective endothelialization and wound healing, we also studied and compared the smooth muscle cell proliferation and morphology on nano-patterned TiO₂ surface layer. For biological experiments, TiO₂ samples (patterned and unpatterned) were prepared on glass cover slip acting as the substrate, by a simple spin coating followed by imprinting and heat treatment steps, to facilitate microscopic examination and biological assay, while the cells exclusively interacted with the TiO₂ surface. The same method of preparation of the TiO₂ surface layer can also be applicable to other types of substrates (e.g., Ti, Ni-Ti alloy, etc.).

2. Experimental Section

2.1. Fabrication and characterization nano-patterned TiO₂

All the precursors were purchased from Sigma Aldrich. Titanium methacrylate solution was prepared by mixing titanium *n*-butoxide, and methacrylic acid (MAA) in a molar ratio of 1:4 to replace all the *n*-butoxy groups. The reaction yielded a yellow solution. To this ethylene glycol dimethacrylate (EDMA), a cross-linker, was added to form TiO₂ resin. Finally, 2 wt% of azobisisobutyronitrile (AIBN), a thermal initiator, was added to the resin to facilitate *in situ* free radical polymerization during imprint lithography. Imprinting of TiO₂ resulted in the formation of a polymer network, which not only trapped the metal atom but also increased the strength of the imprinted structures. Although the TiO₂ surface layer can also be fabricated on substrates other than glass, however, glass was chosen as a substrate in current study to fabricate a surface layer of TiO₂ because of its transparency, which enables high resolution microscopy imaging. Prior to nanoimprinting, the glass substrates and Si molds were cleaned with piranha solution at 140 °C for 2 hours, followed by rinsing with deionized water and blow-drying using a nitrogen gun. The glass substrates were placed in a drying oven to remove any remaining moisture on the surface. The Si molds were treated with 100 µL of perfluorodecyl-trichlorosilane for 15 minutes at 80 °C to reduce their surface energy in order to facilitate a clean demolding after nanoimprinting. The dimensions of substrates used were 2 cm x 2 cm. The types of mold used were 250 nm gratings and wells, both of them had an aspect ratio of 1. TiO₂ resin was spin coated onto the glass substrate at a speed of 3000 rpm for 30 seconds, which resulted in a film of 500 nm thickness. The Si mold, of a smaller size, was placed on top of the film. A 2-step nanoimprinting process was carried out in an Obducat imprinter (Obducat, Sweden). At first, a temperature of 30 °C and pressure of 10 bars was applied for 5 minutes to allow the resist to fill the structures of the mold followed by elevating the temperature to 110 °C for 5 minutes to achieve *in situ* free radical polymerization of the resin. Samples were cooled to room temperature before pressure was release. Subsequently, demolding step was carried out. The yield was found to be ~100%. Finally, the imprinted patterns were heat treated at a temperature of 450 °C for one hour in air to remove organic components. This resulted in an array of TiO₂ nano-gratings and nano-wells. To acquire the images of TiO₂ patterns, a JEOL JSM-6700F field-emission scanning electron microscope (FE-SEM) was used. Schematic diagram of the TiO₂ patterning is shown in Figure S1.

2.2. Endothelial and smooth muscle cell culture

Human umbilical vein endothelial cells (HUVECs) were obtained from Lonza and cultured in Endothelial Cell Growth Medium (EGM-2, Lonza). Human coronary artery smooth muscle cells (SMCs) were obtained from Promocell and cultured in Smooth Muscle Cell Growth Medium-2 with SupplementMix (Promocell). Both cell types were cultured in standard cell culture conditions (37 °C, humidified, 5% CO₂ / 95% O₂ environment) and media was changed every other day.

Cells were passaged at 80-90% confluence by using trypsin (Gibco) and seeded on samples for experiments. Endothelial and smooth muscle cells for all experiments were used between passages 3-5.

2.3. Cytotoxicity analysis of nano-patterned TiO₂ substrates

Cytotoxicity of TiO₂ substrates was analyzed by using AlamarBlue and live/dead assays. For AlamarBlue assay, HUVECs were seeded at 2000 cells/cm² seeding density on glass cover slips, heat-treated, and non-heat-treated TiO₂ samples in 12 well plates and cultured in Endothelial Cell Growth Medium (EGM-2MV, Lonza). At day 3 and day 5, samples were transferred to new 12 well plates and 10% AlamarBlue (Life Technologies) in culture medium was added and incubated for 4 hrs. The redox reaction, in which AlamarBlue is reduced by the cells, was measured by absorbance readings at 540 and 630 nm and percentage reduction of the AlamarBlue dye was calculated according to the formula provided by the vendor. A higher percentage reduction implies a higher number and viability of cells. For the live/dead assay at day 7, endothelial cells were incubated for 45 minutes with 3.3 mM of calcein AM and 1.7 mM of ethidium homodimer-1 (Life Technologies). After incubation, the cells were analyzed with fluorescence microscope (Leica DM IRB) and the images were processed using Image J (NIH).

2.4. Endothelial cell proliferation assay and von Willebrand factor (vWF) staining and scanning electron microscopy imaging

For assessment of cell proliferation, HUVECs were seeded on cover slips, unpatterned and patterned TiO₂ substrates at a seeding density of 3000 cell/cm² in 12 well plates and cultured for 24 hrs in Endothelial Cell Growth Medium (EGM-2MV, Lonza). After 24 hrs, cell proliferation was detected by using Alexa Fluor 488 Click-iT EdU cell proliferation assay kit (Invitrogen). Briefly, the cells were incubated with 10 μM 5-ethynyl-2'-deoxyuridine (EdU) for 4 hrs. Subsequently, the cells were fixed with 4% paraformaldehyde in 1x PBS, permeabilized in 0.1% Triton-X in 1x PBS, and stained for EdU dye according to the kit's protocol. Click-iT EdU Cell Proliferation assay also allows the co-staining of other antibodies along with EdU dye. After staining for EdU, cells were washed twice with 1x phosphate buffered saline (PBS) and blocked with 10% goat serum for 1 hr. After blocking, the cells were incubated with mouse IgG1 anti-Von Willebrand factor (vWF) antibody (Santa Cruz) for 1 hr at room temperature with dilution factor of 1:300. The samples were then incubated with 2.67 μg/ml of Alexa Fluor 546®-conjugated goat anti-mouse antibody (Invitrogen) for 1 hr at room temperature and counterstained with 2 ng/ml 4',6-diamidino-2-phenylindole (DAPI, Sigma-Aldrich) for 30 min at room temperature. EdU incorporation in proliferating cells was determined by fluorescent microscopy. Primary antibodies were diluted in 1% goat serum in 1x PBS while secondary antibodies were diluted in 1x PBS.

For scanning electron microscopy imaging, the HUVECs were cultured on TiO₂ samples for 24 hrs as mentioned above.

Subsequently the cells were fixed with 4% paraformaldehyde and 1% glutaraldehyde (Sigma Aldrich) in 0.1 M sodium cacodylate and 3 mM CaCl₂ buffer, serially dehydrated in ethanol gradient and critical point dried (Blazer CPD 030). The samples were sputter-coated with 20 nm platinum coating before imaging with FE-SEM (JSM-6700F).

2.5. Focal adhesion kinase staining and quantitative characterization

For visualization of vascular endothelial cell focal adhesions (FA), HUVECs were seeded on cover slips, unpatterned and patterned TiO₂ substrates at a seeding density of 5000 cell/cm² in 12 well plates and cultured for 24 hrs in Endothelial Cell Growth Medium (EGM-2MV). After 24 hrs the cells were fixed, permeabilized, and blocked as described in Section 2.4, and stained with rabbit anti-phosphorylated Y397 FAK primary antibody (Abcam) at 1:100 dilution, followed by Alexa Fluor 488®-conjugated goat anti-rabbit IgG antibody (Invitrogen), with nuclei and F-actin counter-stained. For the quantification of FAs, the local contrast of each image was first enhanced using the CLAHE algorithm.²⁶ The images were then converted to binary mode. The "analyze particles" tool in ImageJ (NIH) was used to find the density, elongation and average area of FAs. FA density is defined as the number of focal adhesions per cell. At least 50 cells from three different samples were analyzed for FA size, elongation and density quantification.

2.6. Smooth muscle cell proliferation and cell shape analysis

For the analysis of SMC proliferation and cell shape, SMCs cells were seeded on cover slips, unpatterned and patterned TiO₂ substrates at a seeding density of 3000 cell/cm² in 12 well plates and cultured for 24 hrs in Smooth Muscle Cell Growth Medium-2 with SupplementMix (Promocell). After 24 hrs, SMC proliferation was detected by using the Alexa Fluor® 488 Click-iT® EdU Cell Proliferation assay kit. Briefly, the cells were incubated with 10 μM EdU for 4 hrs. The cells were then fixed, permeabilized, and stained for EdU dye. After staining for EdU, the cells were washed and stained with mouse anti beta-actin primary antibody (Abcam) with 1:500 dilution in 1x PBS followed by 2.67 μg/ml Alexa Fluor 546®-conjugated goat anti-mouse IgG antibody (Invitrogen) staining for 1 hr. Finally the cells were stained with 2 ng/ml DAPI for 30 min.

2.7. Endothelial cell morphometric analysis

To investigate the effect of nano-topography on endothelial cell morphology, F-Actin stained cells were used to analyze cell aspect ratio. ImageJ (NIH) was used to calculate aspect ratio for each cell. Aspect ratio is defined as the ratio between the length and breadth of each cell. At least 50 cells from three different samples were analyzed to measure cell aspect ratio.

2.8. Statistical analysis

Data are presented as mean ± SD. Student's t-test and one-way ANOVA followed by Tukey's test were used to evaluate the statistical significance where indicated. Statistical analysis was performed with quadruplicates in all experiments.

3. Results and discussion

3.1. Characterization of nano-patterned TiO₂ substrates

Heat treatment was carried out to remove organic components and convert the imprinted TiO₂ resin into a continuous TiO₂ surface layer with nanopatterns atop. Figure 1(a) shows the SEM images of TiO₂ nanogratings of 70 nm width after heat-treatment at 450 °C for 1 hour in air. The gratings height was also 70 nm as measured by using FE-SEM cross sectional

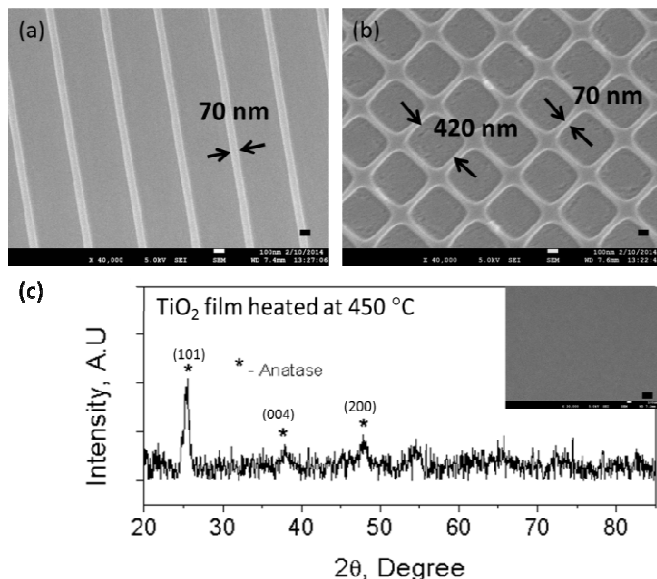


Figure 1: FE-SEM images of (a) 70 nm TiO₂ gratings and (b) 420 nm TiO₂ square wells with 70 nm wall thickness (c) XRD of the heat treated film at 450 °C (inset shows SEM image of blank film). Feature height is 70 nm. (Scale bar=100 nm)

images. Similar heat-treatment yielded 420 nm wide square-wells with wall thickness and height of 70 nm [Figure 1(b)]. The total feature size reduction due to loss of organics was ~70%. Although there was a pattern size reduction, the periodicity and fidelity was still kept the same as the original Si master mold. Pattern size reduction allows the fabrication of sub-100 nm TiO₂ nanostructures. Moreover, this method of patterning is useful for biological studies of oxide materials in this size range, which was previously challenging to fabricate using other lithography methods. XRD study of heat-treated TiO₂ layer shows that anatase phase appears at 450 °C [Figure 1(c)]. The diffraction peaks (101), (004) and (200) of the heat-treated sample were indexed as anatase phase of TiO₂ and found to be in agreement with those in JCPDS Card No. 89-4921. The three crucial parameters for successful imprinting of TiO₂ nanostructures are spin-coating speed, heat-treatment time and temperature. Optimizing these parameters appears to be crucial not only to achieve good imprint quality and yield but also to the integrity of TiO₂ structures after heat-treatment. The spin-coating speed determines the film thickness to be imprinted while the heat-treatment time and temperature determine grain growth and phase of the imprinted TiO₂. It was found that residual layer thickness of slightly less than 400 nm

was ideal to achieve TiO₂ lines of good integrity after heat-treatment.²⁷

Our method has several advantages for nanoimprinting of TiO₂. Firstly, the *in situ* free radical polymerization of TiO₂ resin during imprinting not only rigidly shapes the imprint, but also traps the metal atoms. Furthermore, polymerization reduces the surface energy and strengthens the imprinted structures, which results in ~100% yield after demolding. Secondly, the use of conventional silicon molds in conjunction with liquid metal methacrylate resin results in the achievement of high resolution imprinting over large areas, which is difficult by other methods such as etching of TiO₂ films. More importantly, using this method of fabricating TiO₂ nanostructures, periodic sub-100 nm resolution structures can be achieved due to size reduction of features during heat treatment. To exclude the possibility of serum proteins covering the nano-topography, the integrity of the nano-features were confirmed by incubating the samples in culture media overnight and its subsequent FE-SEM analysis. The incubation of samples in culture media did not affect the surface topography (Figure S1).

3.2. Cytotoxicity analysis of nanopatterned TiO₂ substrates

Heat treatment is performed to remove the organic compounds, which could be toxic for most cells. Unpatterned heat-treated TiO₂ layer, which was imprinted with a pristine Si mold without any topographical pattern, was studied for cytotoxicity. Figure 2 shows phase contrast microscopy images of vascular endothelial cells, showing the cell growth on cover slip control, heat-treated (HT) TiO₂ and non-heat-treated (non-HT) TiO₂ (i.e., thermally polymerized TiO₂ resin). The images were taken at 2 hrs after seeding, at day 3, and at day 5. As can be seen from the Figure 2, cell growth on HT-TiO₂ was on par with that of cover slip control. Initial cell attachment was observed on

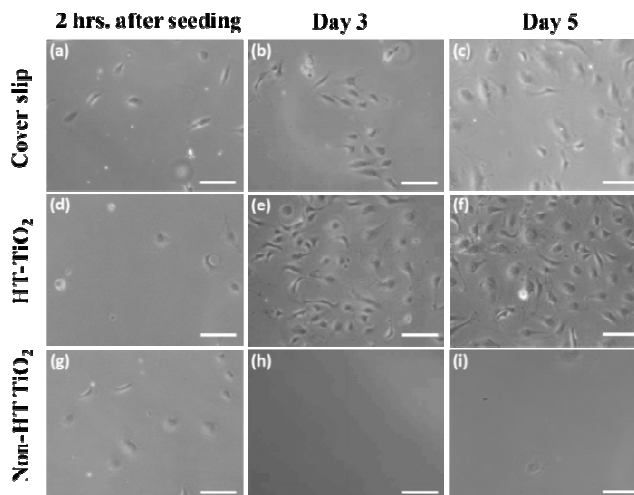


Figure 2: Phase contrast microscopy images of Human Umbilical Vein Endothelial cell (HUVEC) growth on (a-c) cover slip control (d-f) unpatterned heat-treated TiO₂ and (g-i) non-heat-treated TiO₂. The images were taken at 2 hrs after seeding, at day 3, and at day 5. (Scale bar=100 μm)

non-HT TiO₂ samples after 2 hrs of seeding. By day 3, very few cells were observed on non-HT-TiO₂ samples and essentially no cell was observed by day 5. Cell viability on cover slip, non-HT TiO₂ and HT-TiO₂ was measured by using AlamarBlue assay at day 3 and day 5 in culture [Figure 3(a)]. Cell viability was found to be slightly higher on HT-TiO₂ as compared to the glass cover slip control, which implied that the HT-TiO₂ is not cytotoxic and confirmed the results obtained by phase contrast microscopy images. As expected, cells did not show any appreciable growth on non-HT TiO₂ samples. Cytotoxicity of the heat-treated TiO₂ resist was also evaluated by using live/dead assay with cover slip as control. As shown in the Figures 3(b, c), at day 7 in culture, HT-TiO₂ showed cell viability, which was comparable to the cover slip control. Hardly any cells were found on non-HT TiO₂ samples by day 7 (data not shown). Taken together, these results indicate that the

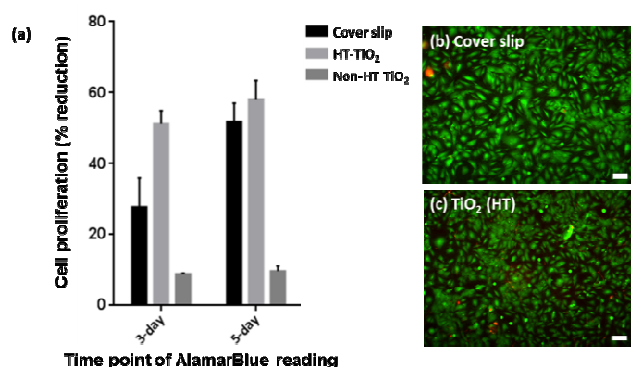


Figure 3: Human Umbilical Vein Endothelial cell (HUVEC) viability as measured by (a) AlamarBlue assay at day 3 and day 5 on glass cover slip, heat-treated TiO₂ (HT-TiO₂) and non-heat-treated TiO₂ (non-HT TiO₂) by incubating cells with AlamarBlue dye for 4 hrs. Live/dead assay at day 7 on (a) cover slip control and (b) heat-treated TiO₂. Green colour shows viable cells while red shows dead cells. (Scale bar=100 μm)

TiO₂ used in this study is non-toxic to cells and it can be used to evaluate the effect of patterned TiO₂ nano-topography on cellular responses.

3.3. Functional marker expression of HUVECs on nanopatterned TiO₂

Von Willebrand factor (vWF) is a functional marker for vascular endothelial cells. HUVECs were stained for vWF to confirm that the vascular endothelial cells are not de-differentiated into fibroblastic-like phenotype and that the cells show vascular endothelial-specific functional marker after growing on patterned HT-TiO₂. As shown in Figure 4, vWF was well expressed by HUVECs on cover slip control, unpatterned TiO₂, TiO₂ nano-wells, and TiO₂ nano-gratings. The results suggest that HUVECs were not de-differentiated on TiO₂ substrates, and the substrates did not alter the functional characteristics of endothelial cells. Moreover, the vascular endothelial cells on TiO₂ nano-gratings were elongated along the direction of gratings.

3.4. Endothelial and smooth muscle cell proliferation

The proliferation of vascular endothelial and smooth muscle cells was measured by EdU incorporation assay. Seeding density and experiment time points for both cell types were kept the same to facilitate comparison of the results between two cell types. As shown in Figure 5(a), vascular endothelial cells showed increased proliferation rate on TiO₂ nanogratings as compared to the cover slip control and unpatterned TiO₂ surface though not statistically significant. Previously, endothelial cells demonstrated decreased proliferation on grating surfaces with decreasing pitch size and their proliferation was significantly lower than planar control.⁸ The data presented in this study suggests that imprinted TiO₂ nanogratings do not lower the proliferation rate of HUVECs as

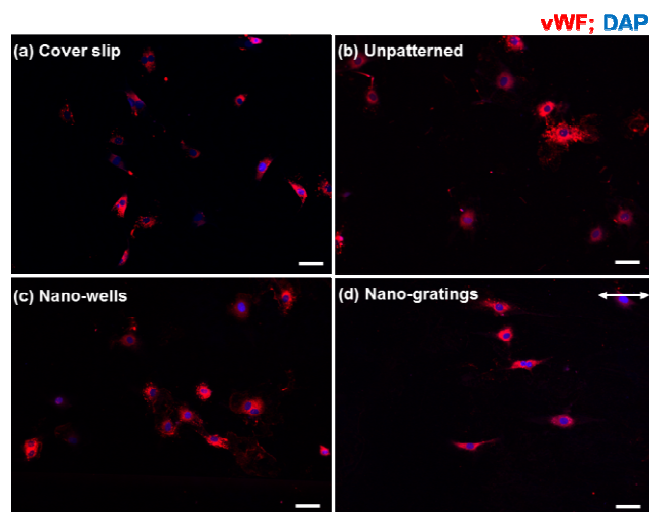


Figure 4: Von Willebrand factor (vWF) expression of human umbilical vein endothelial cell (HUVEC) on (a) cover slip (b) unpatterned TiO₂ (c) TiO₂ nano-wells (d) TiO₂ nano-gratings. Arrow shows the direction of gratings (Scale bar=50 μm)

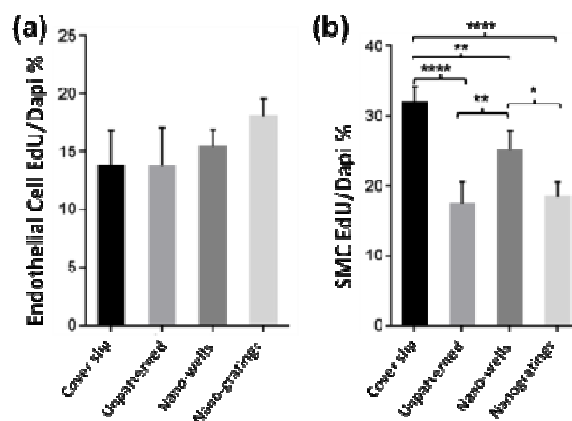


Figure 5: (a) Human umbilical vein endothelial cell (HUVEC) and (b) human coronary artery smooth muscle cell (SMC) proliferation on various topographies as measured by 5-ethynyl-2'-deoxyuridine (EdU) incorporation in the proliferating cells' DNA. *p<0.05; **p<0.01; ***p<0.005; ****p<0.0001

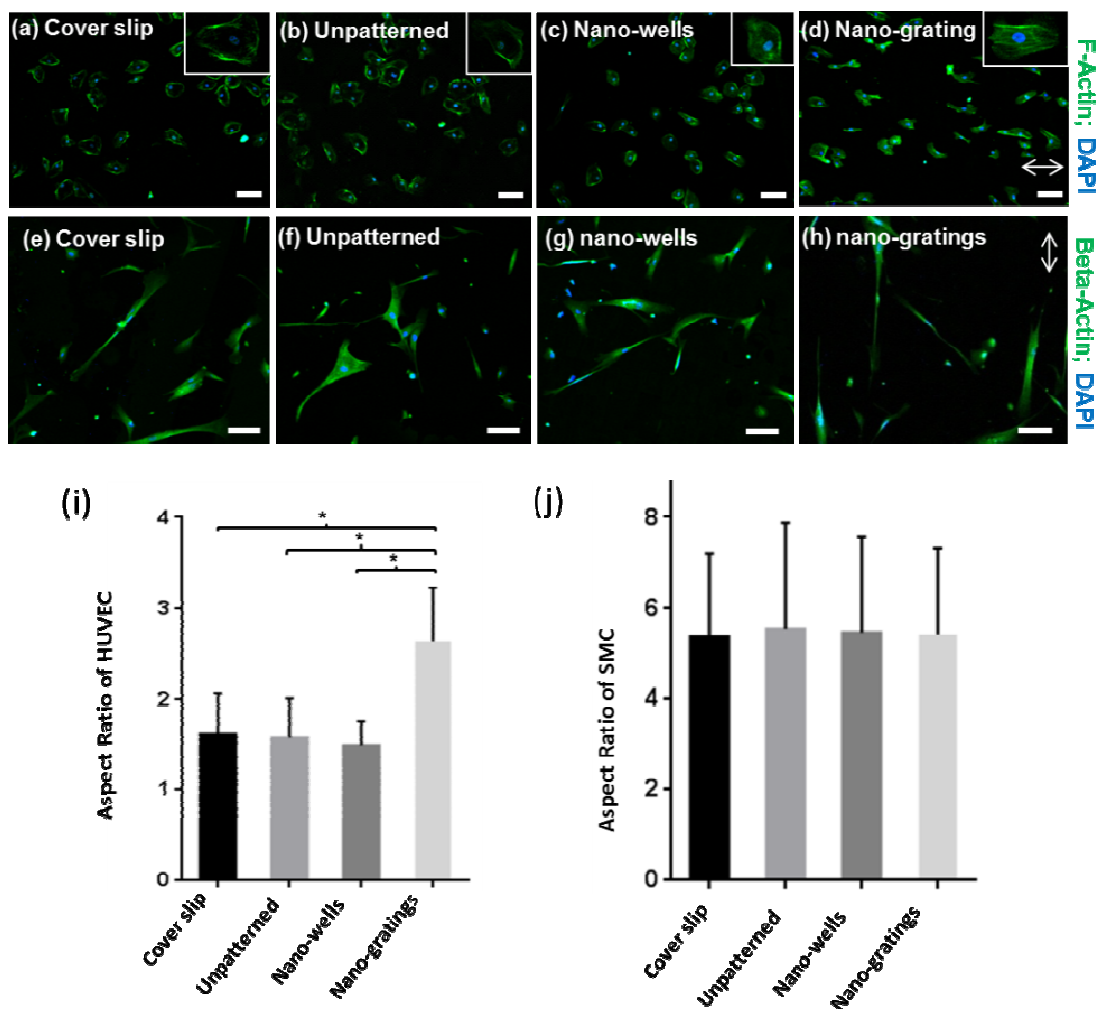


Figure 6: Fluorescent staining of F-actin in HUVECs shows the cell morphology on (a) cover slip control (b) unpatterned TiO₂ (c) TiO₂ nano-wells and (d) TiO₂ nano-gratings. Inset shows a magnified view of the HUVEC cell morphology. Fluorescent staining of beta-actin to visualize the morphology of smooth muscle cells on (e) cover slip control (f) unpatterned TiO₂ (g) TiO₂ nano-wells and (h) TiO₂ nano-gratings. Aspect ratio of (i) Human umbilical vein endothelial cell (HUVEC) and (j) smooth muscle cells on cover slip control and various TiO₂ substrates. Aspect ratio is defined as the ratio between the long axis and short axis of the cells. *p<0.001 (scale bar=100 μm)

compared to the planar control. In fact, the proliferation rate was found to be slightly higher on nanogratings as compared to the cover slip control and unpatterned TiO₂. Nanoimprinted TiO₂, on the other hand, demonstrated a greater impact on the proliferation of SMCs. As shown in the Figure 5(b), SMCs showed a significantly decreased proliferation rate on all TiO₂ surfaces as compared to the cover slip control. Within various TiO₂ surfaces, SMCs showed statistically significant higher proliferation rate on nano-wells as compared to unpatterned TiO₂ and TiO₂ nano-grating. These results reveal that SMCs are able to sense underlying sub-100 nm biophysical cues and respond to it by modulating their proliferation capacity. It has been shown that SMCs proliferation is one of the major causes of restenosis after stent application.^{28, 29} Hence, decreased proliferation rate of SMCs is relevant and desired to resist restenosis. The current findings suggest that nanoimprinted TiO₂ may be utilized to suppress SMCs proliferation and

achieve competitive advantage for the proliferation of endothelial cells.

3.5. Effect of nanoimprinted TiO₂ topography on cell shape

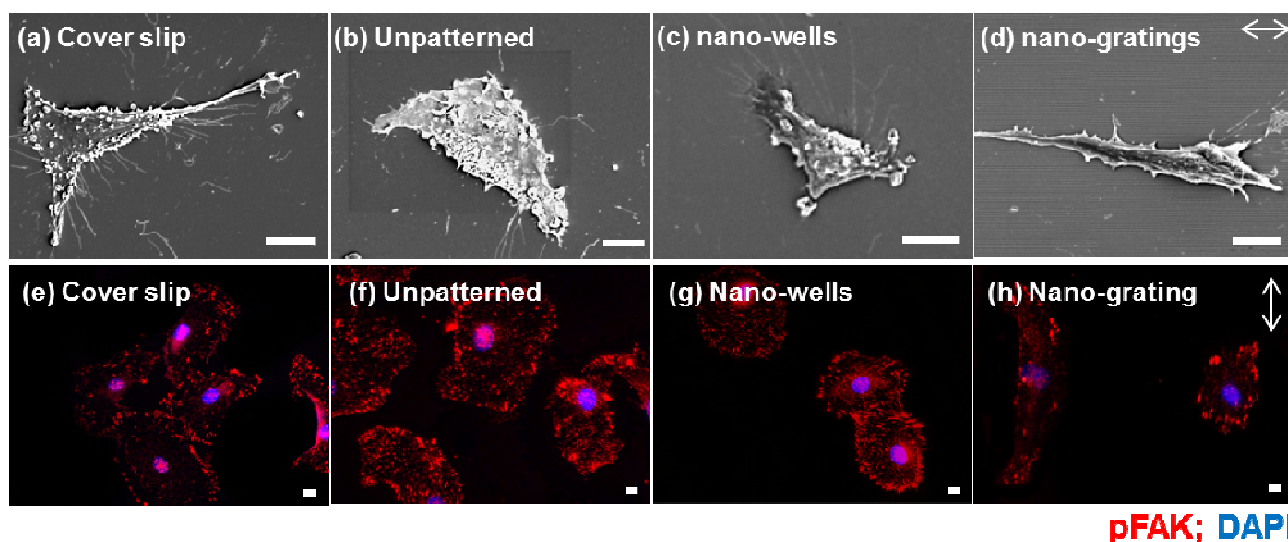
Vascular endothelial cells were stained for actin cytoskeleton to analyze the cell shape. As shown in Figure 6(a-d), endothelial cells showed rounded morphology on unpatterned TiO₂, and TiO₂ nano-wells. On the contrary, on the TiO₂ nano-gratings, endothelial cells assumed a more elongated morphology along the direction of gratings. In addition, smooth muscles cells were stained for beta-actin to visualize the cell shape [Figure 6(e-h)]. The smooth muscle cells had larger area as compared to vascular endothelial cells and they were also aligned along nano-gratings. Similarly, smooth muscle cells did not show and visible trend in cell shape on unpatterned TiO₂ and TiO₂ nano-wells. To further investigate the effect of topography on vascular endothelial and smooth muscle cell shape, morphometric analysis of cell shape was carried out to quantify

the cell aspect ratio. Endothelial cells on nano-gratings and patterned surfaces had significantly higher aspect ratio (long axis : short axis) as compared to the nano-wells and unpatterned surfaces [Figure 6(i)]. In case of smooth muscle cells, no significant differences were found between cell aspect ratio on different topographies [Figure 6(j)]. Smooth cell cells had an aspect ratio of about 5-6 on cover slips, patterned, and unpatterned TiO₂. Endothelial cell orientation and alignment are important processes for the formation of new vessels and during endothelialization. Essential cell processes may be controlled by the changes in cell shape.³⁰ Endothelial cells that line the blood vessel has slightly elongated morphology due to the shear forces applied by the blood flow.³¹ Nano-patterned TiO₂ surface layer could be used to modulate endothelial cell shape by promoting a more native cellular morphology. It is well-known that cell can be aligned and elongated along the axis of micron and sub-micron gratings.^{7, 32} However, there is a lack of understanding on the size threshold that the cells can sense and align themselves accordingly. The proliferation and cell shape analysis shows that HUVECs and SMCs can sense and respond to the gratings and well border as small as 70 nm, by showing significant changes in proliferation and morphological changes.

3.6. Cell-surface interaction, focal adhesion kinase size, distribution and density

The detailed interaction of endothelial cell and patterned surfaces was characterized by scanning electron microscopy (SEM) [Figure 7(a-d)]. The SEM images revealed that the cells are elongated along the nano-gratings. Meanwhile, no trends in cell alignment were observed on unpatterned or nano-wells, on which the cells were randomly spread. More extensive filopodia formation of the HUVEC was observed on cover slips and TiO₂ nano-wells. Endothelial cells were also stained for

phosphorylated focal adhesion kinase (pFAK) to visualize the effect of topography on the size, distribution and density of focal adhesions. As shown in Figure 7(e-h), focal adhesion distribution, size and density were modulated by the underlying TiO₂ nano-topography. HUVECs on unpatterned TiO₂ and TiO₂ nano-wells surfaces had increased number of focal adhesions (FAs) as compared to HUVECs on TiO₂ nano-gratings. FAs were distributed throughout the cytoplasm on unpatterned and TiO₂ nano-wells while FAs were mostly found on the cell periphery, in the case of nano-gratings with the greater density, at the poles of elongated cells [Figure 7(e-h)]. More FAs were observed on unpatterned TiO₂ and TiO₂ nano-wells as compared to the cover slip control and TiO₂ nano-gratings. On cover slip controls, the FAs were mostly located on the cell periphery. Modulation of FAs by patterned TiO₂ topography was also analyzed quantitatively in terms of FAs size, FAs elongation and number of FAs per cell (Figure 8). As shown in Figure 8(a), FA size was significantly lower on unpatterned TiO₂ as compared to glass cover slips, TiO₂ nano-gratings and nano-wells. No significant difference in FA size was found between nano-gratings and nano-wells samples. FA size distribution can provide more useful information about the range of FA sizes found on various substrates. Figure 8(b) shows the distribution of FA sizes. Almost half of the FAs on unpatterned TiO₂ were found to be larger than 3 μm^2 in size as compared to FAs on TiO₂ nano-gratings and TiO₂ nano-wells, where more than 65% of the FAs were larger than 3 μm^2 in size. On both of the patterned TiO₂ topography, FA size distribution was observed to be extended to up to 20 μm^2 size. However, more tight distribution was found on unpatterned TiO₂ and almost no FAs were found beyond 12 μm^2 size. FA size distribution on glass cover slip was found to be similar to unpatterned TiO₂ with slightly less tight FA size distribution. Figure 8(c) shows the elongation of focal adhesions on various



pFAK; DAPI

Figure 7: Scanning electron microscope images of HUVEC cell shape on (a) unpatterned TiO₂ (b) TiO₂ nano-wells and (c) TiO₂ nano-gratings. HUVEC cells are elongated along the direction of gratings. Focal adhesions distribution as visualized by immuno-fluorescence staining of phosphorylated focal adhesions kinase (pFAK) on (e) cover slip control (f) unpatterned TiO₂ (g) TiO₂ nano-wells and (h) TiO₂ nano-gratings. Arrow shows the direction of gratings (scale bar=10 μm)

substrates. On glass coverslip and unpatterned TiO₂, the focal adhesions were not elongated. However, on TiO₂ nano-wells and nano-gratings, the elongation of focal adhesions was significantly higher as compared to unpatterned TiO₂. FA elongation was similar on nano-wells and nano-gratings although the area of focal adhesions was higher on nano-wells. Figure 8(d) shows the formation of FAs in terms of number of FAs found per cell on various substrates. The average number of FAs per cell for TiO₂ nano-gratings were found to be significantly lower as compared to cover slips, unpatterned

TiO₂ and TiO₂ nano-wells. However, no significant difference in terms of focal adhesion density was found between cover slips, unpatterned TiO₂ and TiO₂ nano-wells. These results match with the qualitative observations about focal adhesion density made on the basis of pFAK-stained images [Figure 7(e-h)]. Taken together, the results demonstrate the ability of TiO₂ nano-wells to increase the formation of FAs and the degree of maturation as compared to unpatterned TiO₂. On the other hand, TiO₂ nano-gratings lead the FAs to maturation but the focal adhesion density was found to be the lowest among all the

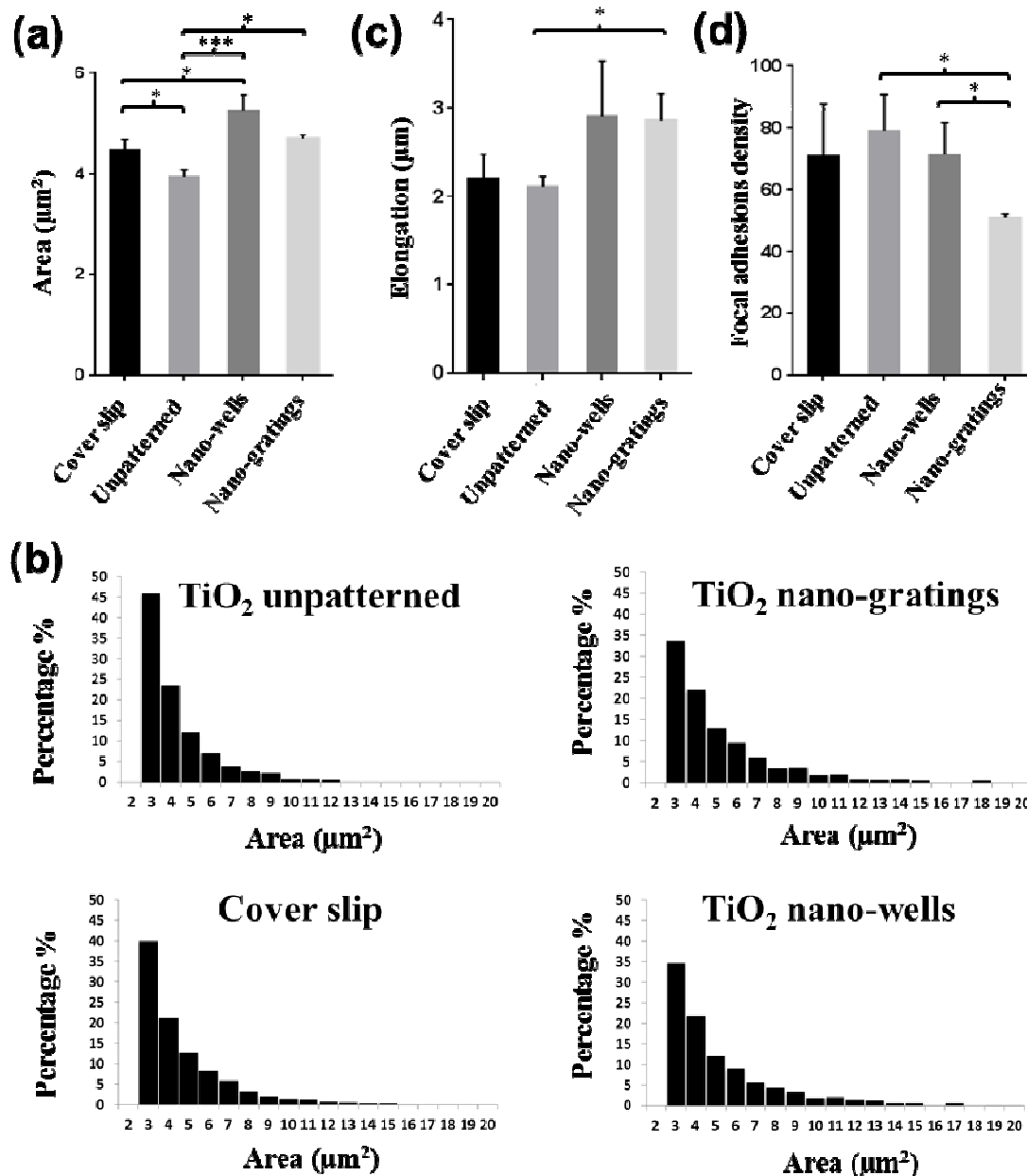


Figure 8: Human umbilical vein endothelial cells (HUVEC) focal adhesion (FA) size and density modulation by nanoimprinted TiO₂. (a) Average FA size on cover slip, unpatterned TiO₂, TiO₂ nano-wells and TiO₂ nano-gratings. (b) Histogram showing the frequency distribution of FAs vs. area on cover slip and unpatterned, nano-wells and nano-gratings. On unpatterned TiO₂, over 45% of the FAs were less than 3 μm^2 in area with much tighter distribution overall while for patterned surfaces, less than 35% of the FAs were lower than 3 μm^2 area with long tail of distribution. (c) FA elongation on cover slip and unpatterned, nano-wells and nano-gratings patterned TiO₂. (d) FA density on cover slip, unpatterned TiO₂, TiO₂ nano-wells and TiO₂ nano-gratings. FA density is defined as the number of focal adhesions per cell. * $p < 0.05$; ** $p < 0.01$; *** $p < 0.005$

analyzed surfaces. The patterned TiO₂ topography seems to play important role in mediating the formation and maturation of the focal adhesions. Previously, Seo *et al.* found that focal adhesion area and formation were higher on patterned square micro-wells topography as compared to unpatterned samples.³³ However, in this study, we found that focal adhesion area was higher on square nano-wells but the focal adhesion density (formation) per cell was slightly lower as compared to unpatterned surface. We have also previously demonstrated that FA area and elongation can be significantly different on micro-gratings and nano-gratings.³⁴ Here we observed that focal adhesions on TiO₂ nano-gratings were elongated along the gratings and usually found on the poles of the cells [Figure 6(h)]. Overall, the current study shows that sub-100 nm topography can have profound effect on FAs as it demonstrates that not only the FA size but also the FA density per cell is strongly influenced by TiO₂ sub-100 nm topography. Focal adhesion size and distribution have been speculated to mediate cell migration. It has been shown that focal adhesions localization, size and density can predict cell migration.³⁵⁻³⁷ Focal adhesion localization on poles of the elongated cells on TiO₂ nano-gratings could modulate the direction of cell migration geared towards the gratings axis. This polar organization is reminiscent of vascular endothelial cells under flow direction.³⁸ The polar organization of focal adhesions also increases the speed cell migration.³⁷ Generally, smaller focal adhesion area and lower focal adhesions density is believed to promote cell migration rates.^{35, 36} Vascular endothelial cells in this study were found to have smaller focal adhesions as compared to cells on TiO₂ nano-wells. The focal adhesions per cell were also significantly lower as compared to the endothelial cells on TiO₂ nano-wells. Endothelial cells with increased cell migration rate may lead to the faster formation of intact endothelium where focal adhesions play an important role in mediating the cell migration rate.³⁷ Based on the finding of previous studies on the link between focal adhesions and cell migration and the current finding of this study about the FAs, it can be speculated that endothelial cells on nano-gratings may have increased cell motility and migration rate which could ultimately enhance the wound healing and re-endothelialization processes and in turn, inhibit restenosis as demonstrated previously on micro-gratings.^{2, 39}

In summary, our data indicate that the TiO₂ resin-based nanoimprinted TiO₂ surface layer is biocompatible and hence for the first time, it can be used to study how the cells respond to biophysical cues in the form of patterned TiO₂ topography in the sub-100 nm range. We have demonstrated that proliferation of HUVECs and SMCs can be modulated by patterned TiO₂ surface layer with optimal surface topographies as biophysical cues. Morphology of the vascular endothelial cells was also shown to be regulated by nanotopography to achieve a more native-like cell shape. Moreover, focal adhesion size and distribution were also modulated by nanoimprinted TiO₂. The study also illustrated the regulation of vascular endothelial and smooth cells functions by patterned TiO₂ features as small as 70 nm and further studies are needed to explore other topographies

in this size regime to achieve more favourable environment for endothelialization. For example, we have clearly demonstrated the suppression of SMCs proliferation with our chosen topographies while these topographies did not reduce the proliferation of endothelial cells. Further studies could be performed to find better topographical surface with biophysical cues that not only suppress the SMC proliferation but also enhance the proliferation of endothelial cells. Similarly, TiO₂ patterned topography was demonstrated to have significant effect on the focal adhesion density and size, which modulates the cell migration during endothelialization and wound healing processes.

4. Conclusions

In this study, we demonstrated that biocompatible titanium dioxide (TiO₂) surface layer could be patterned at high resolution using nanoimprint lithography. AlamarBlue assay and live/dead assay revealed that the as-prepared TiO₂ is not cytotoxic to cells after heat-treatment. Vascular endothelial cells showed similar expression of vWF functional marker on all substrates. Patterned TiO₂ nano-gratings significantly inhibited the proliferation of SMCs as compared to cover slip control and increased the proliferation of endothelial cells as well. Morphometric studies also confirmed that endothelial cells are able to sense patterned TiO₂ gratings as small as 70 nm and found to be elongated along the gratings as measured by cell aspect ratio. Moreover, focal adhesion (FA) size, density and distribution was also significantly modulated by nanoimprinted TiO₂, as the FA density was significantly lower on TiO₂ nano-gratings and the FA size was significantly higher on TiO₂ nano-gratings and nano-wells as compared to unpatterned TiO₂. The study is the first to demonstrate the use of biocompatible nanopatterned TiO₂ layer for cell-topography interaction research to design improved surfaces for better endothelialization.

Acknowledgements

This work was also partially funded by Singapore's A*STAR-ANR fund (1122703037) and the National Research Foundation, Singapore, under its Research Center of Excellence programme administered by the Mechanobiology Institute of Singapore. M. S. M. Saifullah acknowledges A*STAR-JST Project No. IMRE/12-2P0802 and the A*STAR Nanoimprint Foundry Project No. IMRE/13-2B0278 for financial support. R. Muhammad was supported by Singapore International Graduate Award by the A*STAR Graduate Academy.

Notes and references

^a Department of Biomedical Engineering, National University of Singapore, Singapore 117576, Republic of Singapore
Email: eyim@nus.edu.sg

^b Institute of Materials Research and Engineering, A*STAR (Agency for Science, Technology and Research), Singapore 117602, Republic of Singapore

^c Mechanobiology Institute, National University of Singapore, Singapore 117411, Republic of Singapore

^d Department of Surgery, National University of Singapore, Singapore 119228, Republic of Singapore

^e Department of Electrical and Computer Engineering, National University of Singapore, 21 Lower Kent Ridge Road, Singapore 117576, Republic of Singapore

[#] Contributed equally to the work

Electronic Supplementary Information (ESI) available. See DOI: 10.1039/b000000x/

1. G. A. Abrams, S. S. Schaus, S. L. Goodman, P. F. Nealey and C. J. Murphy, *Cornea*, 2000, **19**, 57-64.
2. E. A. Sprague, F. Tio, S. H. Ahmed, J. F. Granada and S. R. Bailey, *Circulation*, 2012, **5**, 499-507.
3. A. Dibra, A. Kastrati, J. Mehilli, J. Pache, R. von Oepen, J. Dirschinger and A. Schomig, *Catheterization and Cardiovascular Interventions*, 2005, **65**, 374-380.
4. S. Brody, T. Anilkumar, S. Liliensiek, J. A. Last, C. J. Murphy and A. Pandit, *Tissue Eng.*, 2006, **12**, 413-421.
5. S. A. Biela, Y. Su, J. P. Spatz and R. Kemkemer, *Acta Biomater.*, 2009, **5**, 2460-2466.
6. L. E. Dickinson, D. R. Rand, J. Tsao, W. Eberle and S. Gerecht, *J. Biomed. Mater. Res. Part A*, 2012, **100A**, 1457-1466.
7. E. K. F. Yim, R. M. Reano, S. W. Pang, A. F. Yee, C. S. Chen and K. W. Leong, *Biomaterials*, 2005, **26**, 5405-5413.
8. S. J. Liliensiek, J. A. Wood, J. Yong, R. Auerbach, P. F. Nealey and C. J. Murphy, *Biomaterials*, 2010, **31**, 5418-5426.
9. S. Choudhary, K. M. Haberstroh and T. J. Webster, *Tissue Eng.*, 2007, **13**, 1421-1430.
10. D. Khang, J. Lu, C. Yao, K. M. Haberstroh and T. J. Webster, *Biomaterials*, 2008, **29**, 970-983.
11. J. Lu, D. Khang and T. J. Webster, *2009 35th Annual Northeast Bioengineering Conference*, 2009, **1**, 362-363.
12. C. C. Mohan, K. P. Chennazhi and D. Menon, *Acta Biomater.*, 2013, **9**, 9568-9577.
13. C. C. Mohan, P. R. Sreerexha, V. V. Divyarani, S. Nair, K. Chennazhi and D. Menon, *J. Mater. Chem.*, 2012, **22**, 1326-1340.
14. F. Variola, J. B. Brunski, G. Orsini, P. Tambasco de Oliveira, R. Wazen and A. Nanci, *Nanoscale*, 2011, **3**, 335-353.
15. J. Lu, M. P. Rao, N. C. MacDonald, D. Khang and T. J. Webster, *Acta Biomater.*, 2008, **4**, 192-201.
16. A. E. Jantzen, H. E. Achneck and G. A. Truskey, *J. Biomed. Mater. Res. Part A*, 2013, **101**, 3181-3191.
17. G. Tepe, J. Schmehl, H. P. Wendel, S. Schaffner, S. Heller, M. Gianotti, C. D. Claussen and S. H. Duda, *Biomaterials*, 2006, **27**, 643-650.
18. D. Stoeckel, A. Pelton and T. Duerig, *Eur. Radiol.*, 2004, **14**, 292-301.
19. A. R. Pelton, V. Schroeder, M. R. Mitchell, X. Y. Gong, M. Barney and S. W. Robertson, *J. Mech. Behav. Biomed. Mater.*, 2008, **1**, 153-164.
20. S. Shabalovskaya, J. Anderegg and J. Van Humbeeck, *Acta Biomater.*, 2008, **4**, 447-467.
21. S. A. Shabalovskaya, *Bio-Med. Mater. Eng.*, 1996, **6**, 267-289.
22. M. F. Maitz and N. Shevchenko, *J. Biomed. Mater. Res. Part A*, 2006, **76**, 356-365.
23. Z. Huan, L. E. Fratila-Apachitei, I. Apachitei and J. Duszczuk, *J. Funct. Biomater.*, 2012, **3**, 349-360.
24. S. H. Lim, M. S. M. Saifullah, H. Hussain, W. W. Loh and H. Y. Low, *Nanotechnology*, 2010, **21**.
25. R. Ganesan, J. Dumond, M. S. M. Saifullah, S. H. Lim, H. Hussain and H. Y. Low, *ACS Nano*, 2012, **6**, 1494-1502.
26. P. S. Heckbert, *Graphics Gems IV*, AP Professional, 1994.
27. R. Ganesan, S. H. Lim, M. S. M. Saifullah, H. Hussain, J. X. Q. Kwok, R. L. X. Tse, H. A. P. Bo and H. Y. Low, *J. Mater. Chem.*, 2011, **21**, 4484-4492.
28. S. O. Marx, H. Totary-Jain and A. R. Marks, *Circulation*, 2011, **4**, 104-111.
29. M. R. Bennett, S. Anglin, J. R. McEwan, R. Jagoe, A. C. Newby and G. I. Evan, *J. Clin. Invest.*, 1994, **93**, 820-828.
30. R. Singhvi, A. Kumar, G. P. Lopez, G. N. Stephanopoulos, D. I. Wang, G. M. Whitesides and D. E. Ingber, *Science*, 1994, **264**, 696-698.
31. M. J. Levesque and R. M. Nerem, *J. Biomech. Eng.*, 1985, **107**, 341-347.
32. E. K. F. Yim, E. M. Darling, K. Kulangara, F. Guilak and K. W. Leong, *Biomaterials*, 2010, **31**, 1299-1306.
33. C. H. Seo, K. Furukawa, K. Montagne, H. Jeong and T. Ushida, *Biomaterials*, 2011, **32**, 9568-9575.
34. B. K. K. Teo, S. T. Wong, C. K. Lim, T. Y. S. Kung, C. H. Yap, Y. Ramagopal, L. H. Romer and E. K. F. Yim, *ACS Nano*, 2013, **7**, 4785-4798.
35. D.-H. Kim and D. Wirtz, *Faseb J.*, 2013, **27**, 1351-1361.
36. M. A. Wozniak, K. Modzelewska, L. Kwong and P. J. Keely, *Biochim. Biophys. Acta*, 2004, **1692**, 103-119.
37. G. M. Artmann and S. Chien, *Bioengineering in Cell and Tissue Research*, Springer, 2008.
38. S. Li, P. Butler, Y. Wang, Y. Hu, D. C. Han, S. Usami, J. L. Guan and S. Chien, *Proc Natl Acad Sci U S A*, 2002, **99**, 3546-3551.
39. W. Casscells, *Circulation*, 1992, **86**, 723-729.

Journal Name

RSCPublishing

ARTICLE